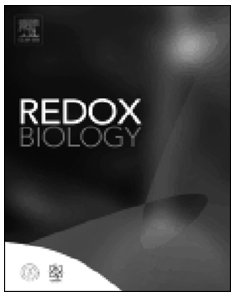

Basal oxidation of conserved cysteines modulates cardiac titin stiffness and dynamics

Elías Herrero-Galán, Inés Martínez-Martín, Cristina Sánchez-González, Natalia Vicente, Elena Bonzón-Kulichenko, Enrique Calvo, Carmen Suay-Corredera, Maria Rosaria Pricolo, Ángel Fernández-Trasancos, Diana Velázquez-Carreras, Claudio Badía Careaga, Mahmoud Abdellatif, Simon Sedej, Peter P. Rainer, David Giganti, Raúl Pérez-Jiménez, Jesús Vázquez, Jorge Alegre-Cebollada

PII: S2213-2317(22)00078-7

DOI: https://doi.org/10.1016/j.redox.2022.102306

Reference: REDOX 102306

To appear in: *Redox Biology*

Received Date: 10 February 2022

Revised Date: 24 March 2022

Accepted Date: 25 March 2022

Please cite this article as: Elí. Herrero-Galán, Iné. Martínez-Martín, C. Sánchez-González, N. Vicente, E. Bonzón-Kulichenko, E. Calvo, C. Suay-Corredera, M.R. Pricolo, Á. Fernández-Trasancos, D. Velázquez-Carreras, Claudio.Badí. Careaga, M. Abdellatif, S. Sedej, P.P. Rainer, D. Giganti, Raú. Pérez-Jiménez, Jesú. Vázquez, J. Alegre-Cebollada, Basal oxidation of conserved cysteines modulates cardiac titin stiffness and dynamics, *Redox Biology* (2022), doi: https://doi.org/10.1016/j.redox.2022.102306.

Basal oxidation of conserved cysteines modulates cardiac titin stiffness and dynamics

Elías Herrero-Galán[1,¶,*], Inés Martínez-Martín[1,¶], Cristina Sánchez-González[1], Natalia Vicente[1], Elena Bonzón-Kulichenko[1,2], Enrique Calvo[1,2], Carmen Suay-Corredera[1], Maria Rosaria Pricolo[1], Ángel Fernández-Trasancos[1], Diana Velázquez-Carreras[1], Claudio Badía Careaga[1], Mahmoud Abdellatif[3], Simon Sedej[3,4,5], Peter P. Rainer[3,5], David Giganti[6], Raúl Pérez-Jiménez[7,8], Jesús Vázquez[1,2], Jorge Alegre-Cebollada[1,*]

[1] Centro Nacional de Investigaciones Cardiovasculares (CNIC), Madrid, Spain

[2] CIBER de Enfermedades Cardiovasculares (CIBERCV), Madrid, Spain

[3] Division of Cardiology, Medical University of Graz, Graz, Austria

[4] Faculty of Medicine, University of Maribor, Maribor, Slovenia

[5] BioTechMed Graz, Graz, Austria

[6] Department of Biochemistry & Molecular Pharmacology and Institute for Systems Genetics, NYU Langone Health, New York, New York, United States

[7] CIC nanoGUNE BRTA, San Sebastian, Spain

[8] Ikerbasque Foundation for Science, Bilbao, Spain

[¶] EHG and IMM contributed equally and are joint first authors.
* EHG and JAC are co-corresponding authors: elias.herrero@cnic.es; jalegre@cnic.es (Twitter: @AlegreCebollada)

ABSTRACT

Titin, as the main protein responsible for the passive stiffness of the sarcomere, plays a key role in diastolic function and is a determinant factor in the etiology of heart disease. Titin stiffness depends on unfolding and folding transitions of immunoglobulin-like (Ig) domains of the I-band, and recent studies have shown that oxidative modifications of cryptic cysteines belonging to these Ig domains modulate their mechanical properties *in vitro*. However, the relevance of this mode of titin mechanical modulation *in vivo* remains largely unknown. Here, we describe the high evolutionary conservation of titin mechanical cysteines and show that they are remarkably oxidized in murine cardiac tissue. Mass spectrometry analyses indicate a similar landscape of basal oxidation in murine and human myocardium. Monte Carlo simulations illustrate how disulfides and S-thiolations on these cysteines increase the dynamics of the protein at physiological forces, while enabling load- and isoform-dependent regulation of titin stiffness. Our results demonstrate the role of conserved cysteines in the modulation of titin mechanical properties *in vivo* and point to potential redox-based pathomechanisms in heart disease.

INTRODUCTION

The passive mechanical properties of cardiomyocytes, such as stiffness, are fundamental for the normal physiology of the heart, and their dysregulation contributes to deficits in the mechanical activity of the myocardium in different forms of heart failure [1], for instance following myocardial infarction [2] or in diabetic patients [3]. A major source of passive stiffness in cardiomyocytes is titin, a giant protein in sarcomeres that also provides structural support and mechanosensing functions (**Figure 1A**) [4-6]. The functional relevance of titin is exemplified by the fact that truncating variants in the titin gene (*TTN*) are the main cause of dilated cardiomyopathy (DCM), a disease that is the most frequent trigger of heart failure in the young and of heart transplantation worldwide [7-11].

The mechanical properties of titin are exquisitely modulated both transcriptionally through specific alternative mRNA splicing [12, 13], and posttranslationally via phosphorylation [14]. However, these two mechanisms alone fail to capture the full range of titin mechanical adaptations, showing our incomplete understanding on how the stiffness of cardiomyocytes is affected by biochemical signals targeting titin [2]. The mechanical properties of titin stem from force-dependent conformational changes of the extensible I-band region of the protein (**Figure 1A**). These conformational changes include extension and entropic recoil of the serially linked immunoglobulin-like (Ig) domains and the random-coil N2Bus and PEVK regions, and Ig domain unfolding and refolding transitions [15]. Interestingly, the I-band of titin is rich in cysteine residues, many of which appear at structurally conserved positions within Ig domains [16, 17]. *In vitro* experiments have shown that oxidation of these cysteines has major mechanical consequences. For instance, disulfide bonds established by the triad of structurally conserved cysteines B, F and G in Ig domains stiffen titin via reduction of the protein contour length [18] (**Figure 1B)**, while S-thiolation of cysteines 47 and 63 leads to titin softening through Ig folding inhibition [19] (**Figure 1C**).

Here, we have examined the *in vivo* function of this group of structurally conserved cysteines whose oxidative modification has been suggested to modulate the mechanical properties of titin on the basis of *in vitro* evidence [17]. Our results show that basal cysteine oxidations modulate titin mechanics in the myocardium, supporting the functional relevance of altered titin modifications under oxidative stress conditions [20, 21].

RESULTS

Evolutionary conservation of titin mechanical cysteines

In the light of the potential physiological relevance of titin's mechanical cysteines, we first explored their evolutionary conservation by aligning the available titin sequences from 36 species of vertebrates [22] (**Supplementary File S1**). The vast majority of cysteine positions in human titin show more than 95% occupancy in the sequence alignment (i.e. sequence gaps do not typically appear at alignment positions occupied by cysteines, **Supplementary Figure S1A,B**), which shows the robustness of our evolutionary conservation analyses. We present the percentage of evolutionary conservation for all cysteines belonging to Ig domains of human titin in **Figure 1D**. This figure is built from a sequence alignment of both I- and A-band Ig domains of human titin (y-axis) [18], in which we highlight every cysteine position colored according to their evolutionary conservation. We found that cysteines B, F and G in Ig domains show 98% mean evolutionary conservation (**Figure 1E**) and cysteines 47 and 63 are also highly conserved (94% mean evolutionary conservation, **Figure 1E**). These five structurally conserved cysteines are more evolutionary conserved than cysteines appearing in other positions in Ig domains (97% *vs* 89% mean evolutionary conservation, **Figure 1F**). The N2Bus region also contains cysteines that can stiffen titin through disulfide bond formation [23], albeit they are less evolutionary conserved than Ig domain cysteines (53% mean conservation, **Figure 1F, Supplementary Figure S1C**). In summary, the significant conservation of titin's mechanical cysteines throughout evolution supports their importance for the biological function of the protein.

Titin cysteines are oxidized in basal conditions

Beyond the remarkable conservation of I-band titin's cysteine residues and their role in the evolution of the protein in vertebrates [22], the *in vivo* relevance of redox mechanical modulation of titin is supported by limited data on the global oxidation of the protein [20, 21, 24-27], the effects of redox-active molecules on striated muscle mechanics [19, 23, 28, 29], and the disulfide-compatible location of the majority of structurally conserved cysteines of titin [18, 30]. However, the extent and location of native titin oxidations, particularly in human titin, remain largely unexplored. Recently, Loescher *et al.* have shown using mass spectrometry that under oxidative insults *ex vivo* and *in vivo*, induced oxidations preferentially target cysteines in the distal I-band region of murine cardiac titin through a mechanism involving protein unfolding [20]. However, our grasp of the range of redox modulation of titin remains limited since it is unknown whether and to what extent titin cysteines are oxidized also in basal, non-oxidative conditions. Whether oxidations target human titin is also unknown.

To examine basal oxidation of titin, we first developed a SDS-PAGE-based assay to define experimental conditions that minimize potential artifactual oxidations that can result from sample manipulation or inefficient thiol derivatization [31]. The assay exploits thiol chemistry reactions to block reduced cysteines with an alkylating agent and label reversibly oxidized cysteines with the fluorophore monobromobimane (mBBr) (**Figure 2A**) [32]. Titin oxidation was directly quantified after running 3.5% acrylamide SDS-PAGE gels, in which the slowest migrating band is contributed by several titin isoforms in the tissue [33, 34]. We verified that the mBBr fluorescence signal of titin cysteines is linearly dependent on the amount of lysate analyzed (**Figure 2B, Supplementary Figure S2A**) and used Coomassie staining (**Figure 2C, Supplementary Figure S2A**) to get normalized oxidation measurements that are independent of the amount of protein loaded on the gel (**Figure 2D**). The initial alkylation is done in denaturing conditions to block all reduced cysteines. This step needs to be fast and complete to limit artifactual oxidation signal. We chose N-ethylmaleimide (NEM) as the alkylating agent because of its superior reaction kinetics and its high solubility in aqueous buffers [26, 31]. Using readily available cardiac samples from adult mice, we found that titin oxidation signal plateaus at NEM

concentrations above 5 mM (**Figure 2E**), suggesting that these conditions result in minimal artifactual oxidation. To further ensure efficient thiol blockage, in all our subsequent experiments we perfused myocardial tissue with 50 mM NEM immediately after sacrifice. The same high NEM concentration was kept during lysis. As an additional preventive measure, we subtracted the mBBr signal of samples not incubated with DTT to account for potential reduced thiols refractory to NEM blockage (see Methods). Using our in-gel mBBr fluorescence assay, we observed that the extent of reversible cysteine oxidation of titin is ~4 times higher than that of myosin, a partner protein of titin in the sarcomere (**Figure 2F, Supplementary Figure S2B**, to allow comparison, oxidation signals are normalized by the density of cysteines of both proteins, see Methods), confirming that a fraction of titin cysteines are constitutively oxidized in cardiac tissue.

Preferential oxidation of I-band cysteines

To characterize the landscape of reversible titin cysteine oxidations, we resourced to mass spectrometry (MS). In this set of experiments, we focused on myocardial samples from P0 newborn mice because they contain a high proportion of the cysteine-rich N2BA titin isoform [18, 35] and therefore provide better cysteine coverage (**Supplementary Figure S3**). Fluorescent titin bands were sliced from SDS-PAGE gels and treated with trypsin. The resulting peptides were subjected to LC-MS analysis and MS/MS spectra were searched against a mouse proteome database. As expected from the full titin band separation in 3.5% SDS-PAGE gels, 79 ± 1% (3 samples from different whole mouse hearts) of the identified species corresponded to titin-derived peptides, even when using a relaxed identification criterion (5% False Discovery Rate, FDR) (**Figure 3A**). Titin coverage in these searches was 33±3% (**Figure 3B**). To maximize the coverage of cysteine peptides, we followed an alternative, more targeted strategy [36]. Since most detected peptides in the search against the full proteome originate from titin, we repeated the searches against a database containing only titin and all identified cysteine peptides were validated using Vseq [37]. Similar to the in-gel fluorescence method, we excluded mBBr-derivatized peptides

when also detected in –DTT control samples, resulting in a final 45% aggregated cysteine coverage at a FDR<2% (see Methods).

In the MS experiments, we detect reduced and oxidized cysteines from the mass shifts associated to NEM and mBBr modifications, respectively (**Figure 2A**). To obtain a global picture of detected cysteine oxidations, we have calculated a Redox Identification Index (RII) from the number of events in which each cysteine is detected as reduced or oxidized in our samples (see Methods). RII ranges from -1 to 1; these extreme values are given to cysteines that are only detected as reduced or oxidized, respectively. Although RII is a semiquantitative parameter that is not intended to quantify the net oxidation of each specific cysteine position, RII can describe the general landscape of identified cysteine oxidations building on the conserved location of titin mechanical cysteines (**Figure 1B-E**). **Figure 3C** shows RII values for each cysteine position in the alignment of the Ig domains of murine titin. RII data show that titin cysteines of the mechanically active I-band are more frequently detected as oxidized than those belonging to the A-band (**Figure 3D**). In addition, cysteines of the disulfide-competent triad BFG (in particular cysteines F and G) are detected as oxidized more frequently than other cysteines in titin (**Figure 3C,E,F, Supplementary Table S1**). Unfortunately, we did not detect cysteine-containing peptides from the N2Bus region, so its native oxidation state could not be studied.

Titin oxidation in human hearts

We next examined the landscape of cysteine oxidation in human cardiac titin using left ventricular snap-frozen samples from 2 non-transplanted, non-failing donor hearts. The proportion of N2BA titin in adult human left ventricle is 30% [1], which ensures a good coverage of mechanically active, conserved cysteines [18]. The human samples were processed and analyzed following the same approach used for mouse samples. 74±3% of identified peptides were derived from titin when the MS/MS search was done against the human proteome database at a 5% FDR (**Figure 3G**). In these searches, titin coverage was 37±6% (**Figure 3H**). As in experiments using mouse samples, we ran targeted searches against a database containing only human titin and the resulting

cysteine peptides were validated with Vseq. mBBr-derivatized peptides also detected in –DTT samples were excluded from analysis, leading to a final 39% aggregated cysteine coverage at a FDR<2%. As in murine titin, cysteines of the I-band are more frequently detected as oxidized than those of the A-band (**Figure 3I,J**) and the RII of structurally conserved cysteines in Ig domains tends to be higher than that of non-structurally conserved cysteines (**Figure 3I,K, Supplementary Table S1**). Similar to results with murine samples, cysteine F shows the highest RII among disulfide-competent positions, although in human samples the I-band-specific cysteine 47 has the highest RII among the structurally conserved cysteines (**Figure 3I,L, Supplementary Table S1**). In one of the human samples, we detected two cysteines belonging to the N2Bus region (Cys4083 was detected as reduced, and Cys4124 was found both in oxidized and reduced states). In summary, MS results indicate that reversible oxidations are also present in native titin from human myocardium.

Modulation of titin mechanics by redox modifications

Our results show that evolutionary and structurally conserved cysteines of the I-band of titin are oxidized *in vivo*. We find reversible oxidations both in disulfide-competent cysteines and in unpaired cysteines that can establish S-thiolation adducts. These modifications have been proposed to induce opposite mechanical effects [17-19], an observation that may contribute to explain the different modulation of titin-based striated muscle stiffness under specific redox challenges [19, 20, 23, 28, 29]. To illustrate the range of regulation of titin mechanics by cysteine oxidation, we built on previous Monte Carlo simulations [19] to integrate all known mechanical effects of redox posttranslational modifications in titin Ig domains. These include reduction of contour length by disulfide bonds [18], higher unfolding and folding rates of disulfide-containing domains [18, 38], and higher unfolding rates and hampered folding of S-thiolated domains [19]. In our simulations, we tuned unfolding and refolding rate constants to qualitatively reproduce the recently described unfolding/folding dynamics of native titin [33] (**Supplementary Note S1, Supplementary Figure S4A**). In the simulations, a virtual human I-band titin is subject to 1 Hz triangular force pulses between 0 and a predefined peak force, and the resulting length of titin is

measured (**Figure 4A,B**). During the extension/relaxation cycles, titin domains unfold and refold stochastically according to their folding and unfolding rates, which are dependent on their redox state. At t=0 s, all domains are folded and, as the simulations proceed, a fraction of domains transition to the unfolded state resulting in longer titin lengths (**Figure 4C,D**). The simulation time was long enough to reach steady-state lengths at all peak forces (**Figure 4C,D, Supplementary Figure S4B-E**).

Simulations of the canonical N2BA titin at a low peak force of 10 pN show that disulfides and S-thiolations result in longer titin lengths (i.e. lower stiffness) (**Figure 4C**), while at a peak force of 100 pN, the effect of disulfides reverses leading to overall titin stiffening (**Figure 4D**). At this high peak force, S-thiolation maintains its softening effect. Additive mechanical modulation occurs if both oxidative modifications are present in titin simultaneously (**Figure 4C,D)**. To have a broader view of the extent of titin softening/stiffening induced by redox modifications, we did simulations at a range of peak forces and calculated the ratio of titin steady-state peak lengths between the oxidized and the reduced conditions. Results show that the softening effect of S-thiolation remains fairly constant, whereas at 50-80 pN peak force, the contribution of disulfides transitions from softening to stiffening (**Figure 4E, Supplementary Figure S4F**). This dual behavior stems from the fact that disulfides favor mechanical unfolding of Ig domains (softening effect), while also reducing the contour length of unfolded domains and increasing folding rates (stiffening effects). At low peak forces in which Ig domain unfolding rates are low, the softening effect is more prominent; while at high peak forces in which Ig unfolding is more frequent, the stiffening effects prevail. Beyond modulation of steady-state titin stiffness, our simulations also illustrate that both disulfides and S-thiolations induce a more dynamic state of titin by favoring Ig domain unfolding reactions, particularly at low forces (**Figure 4F, Supplementary Figure S4G**).

In the human heart, the short N2B isoform is expressed to higher levels than the longer and softer N2BA [1, 39]. Since alternative splicing occurs at the region of titin with the highest density of

cysteines (**Figure 1D**), we also ran Monte Carlo simulations for the N2B isoform of titin. In contrast to the results obtained with N2BA, we find that disulfides do not induce softening of N2B titin at any peak force (**Figure 4G, Supplementary Figure S4H-N**). Interestingly, S-thiolation softens N2B titin to a greater extent (20% *vs.* 10% for N2BA titin at 50 pN peak force, **Figure 4E,G**), reflecting the higher density of S-thiolation-competent Ig domains in N2B (**Supplementary Table S2**). For the same reason, the extent of modulation of titin dynamics by redox modifications is also different in N2B and N2BA titins (**Figure 4H, Supplementary Figure S4O**), although in both isoforms oxidations increase protein dynamics by favoring more Ig domain unfolding.

Our MS results were scarce with regards to the oxidation state of the cysteines in the N2Bus region of titin. Monte Carlo simulations show that potential disulfides in the N2Bus [23] would boost the overall stiffening effect of this redox modification, especially in the short N2B isoform (**Supplementary Figure S4P,Q**). Indeed, under conditions in which N2Bus cysteines form disulfides, disulfides always stiffen titin. Taking together all the results from the Monte Carlo simulations, we conclude that reversible redox modifications have profound effects in the mechanics and dynamics of titin, in a manner that is highly dependent on the specific modification, the isoform of titin and the applied load.

DISCUSSION

The high nucleophilicity of the thiol side chain makes cysteine the most reactive protein amino acid. In addition, cysteine residues are sensitive to irreversible oxidation, which can result in protein aggregation and degradation [40]. As a consequence, proteins tend to include cysteine only if the associated functional benefits compensate the risks stemming from its peculiar physicochemical properties. Indeed, cysteine is among the least frequent but most conserved residues in proteins [41], reflecting key functional roles including configuration of enzyme active sites or metal chelation sites [42-44], establishment of disulfide bonds [38], deployment of electron transport systems [45], or as redox sensors [46]. Although several *in vitro* experiments

over the last years have shown that cysteine oxidation is a strong modulator of titin mechanics, evidence that such modulation is functionally relevant *in vivo* has been lacking [17]. Our results showing that titin is oxidized in basal conditions both in mice and in humans, together with the recent observation that murine titin cysteines are particularly sensitive to oxidative stress challenges [20], demonstrate the *in vivo* relevance of these mechanisms of mechanical modulation.

In vitro, conserved cysteines B, F and G can be induced to form disulfide bonds that alter the nanomechanics of the parent Ig domains [18, 22]. Hence, a plausible scenario is that equivalent disulfides are present naturally in native titin as mechanical rheostats. This view has been traditionally considered unlikely taking into consideration the reducing environment of the cytosol in which sarcomeres are located [23, 30]. However, our biochemical and MS results strongly support the existence of disulfides in titin in basal conditions (**Figures 2 and 3**), which adds to the increasing pool of evidence that redox compartmentalization of cardiomyocytes is more complex than anticipated [47]. In this regard, future research will aim at identifying the biochemical systems responsible for disulfide formation in titin [48-50], and whether equivalent constitutive oxidations target other proteins in the sarcomere [18, 21, 51-53].

Our results indicate that titin I-band cysteines that cannot establish disulfide bonds, such as conserved Cys47, can also be oxidized in basal conditions. By integrating current knowledge on the mechanical effects of cysteine oxidations obtained at the single-molecule level, our Monte Carlo simulations have allowed us to explore the range of oxidative mechanical modulation of titin (**Figure 4**). The simulations suggest that the extent and direction of mechanical modulation depends on the specific titin isoform, the biochemical nature of the oxidative modification (disulfide *vs* S-thiolation, as nicely demonstrated experimentally in [20]) and the range of mechanical load experienced by titin. Two observations stemming from the Monte Carlo simulations are relevant for the redox modulation of titin mechanics at physiologically relevant forces, which are generally assumed to be no higher than 10 pN/titin molecule [15, 54-56]. First,

due mainly to increased Ig unfolding rates, oxidations render the titin filament much more dynamic, up to one order of magnitude at low forces (**Figure 4F,H**). More frequent Ig unfolding can change the landscape of interactors and prime residues for phosphorylation [20], resulting in modulation of titin-based mechanosignaling [1], whereas high folding rates enabled by disulfide bonds can sustain titin's contribution to active muscle contraction [33, 54, 57]. Monte Carlo simulations also illustrate that disulfides can result both in stiffening or softening of titin (**Figure 4E,G**), a consequence of the opposing mechanical effects of disulfides on contour length and the (un)folding rates of Ig domains. This observation, together with the softening effects of S-thiolation, can reconcile seemingly contradictory results of experiments using muscle preparations. For instance, treatment of human cardiomyocytes with the reducing enzyme thioredoxin results in drops in passive tension during oscillatory changes in length [23] while incubation with DTT results in increased passive tension during stepwise length increases [19]. Similar DTT incubations also increase passive tension of rat and human skeletal fibers [29]. Regarding oxidative modifications, treatment of mouse cardiac muscle with H_2O_2 induces increased passive tension in oscillatory protocols [28], whereas specific S-thiolation reactions lead to softening during stepwise extension of human cardiomyocytes [19, 20], an effect also observed in human and rat skeletal muscle [29]. Interestingly, specific induction of disulfides by treatment with protein disulfide isomerase leads to myocyte stiffening, suggesting that the stiffening effect of disulfides prevails under the experimental conditions tested [20].

Overall, our results show that the redox state of conserved cysteines of the I-band of titin is an important modulator of titin mechanics in basal conditions (**Figure 5**). Indeed, our simulations illustrate that the range of titin mechanical modulation achieved by redox posttranslational modifications can be ample, particularly for the induction of more dynamic states of the protein that can influence mechanosignaling cascades. In this context, we speculate that altered redox signaling may cause titin mechanical dysfunction during disease [21, 52], for instance contributing to myocardial stiffening following myocardial infarction [2, 20].

METHODS

Human subject research

Human subject research was carried out in accordance with principles outlined in the Declaration of Helsinki. Procedures for procurement of human left ventricular tissue from 2 non-failing donor hearts that were not used for transplantation were approved by the Ethical Committee of the Medical University of Graz (28-508 ex 15/16) and the *Instituto de Salud Carlos III* (CEI PI 65_2017-v1). Upon ice-cold cardioplegia, cardiac biopsies were harvested from the left ventricular free wall, quickly frozen in liquid nitrogen and stored at -80°C. Both hearts had echocardiographic evidence of preserved ejection fraction (>50%) and a clinical history that was free of cardiac abnormalities.

Animal research

All post-mortem animal samples used in this work were from CD1 mice housed and maintained in the animal facility at the CNIC (Madrid, Spain) in accordance with Spanish and European Legislation (Directive 2010/63/EU amended by Regulation EU 2019/1010).

Cysteine conservation analysis

The longest currently available titin sequences for the 37 species reported in [22] were aligned using Clustal Omega, with the only exception of chicken, for which no titin sequence with enough coverage was found in Uniprot, GenomeNet or NCBI databases. Sequence identification codes are listed in **Supplementary Note S2**. Conservation values for all cysteine positions in the human titin sequence (Uniprot Q8WZ42) were obtained as percentages of conservation not considering gaps in the alignment. The alignment and homology models of titin Ig domains of human titin have been published before [18]; alignment of mouse titin Ig domains appearing in Uniprot was obtained similarly using Clustal Omega (**Supplementary Note S3**). These Ig domain alignments were used to classify titin cysteines for structural conservation and mass spectrometry analyses.

In-gel determination of reversibly oxidized thiols

Our protocol for in-gel determination of reversibly oxidized thiols was adapted and optimized from previous reports [22, 32]. Protein extracts were obtained by cryopulverization of myocardial tissue followed by homogenization in sample buffer (50 mM Tris-HCl, 10 mM EDTA, 3% SDS, pH 6.8; 40 µl per mg of tissue) containing 50 mM NEM, unless indicated otherwise. Samples were run on SDS-PAGE gels (3.5% for analysis of titin, 12% for other proteins) in the absence of reducing agents. Following electrophoresis, oxidized thiols were reduced by incubation of the gel with 10 mM DL-dithiothreitol (DTT) (Sigma-Aldrich) in 50 mM ammonium bicarbonate, pH 8.8 at 60ºC. After 3 washes of 20 min with sample buffer, the newly reduced thiols were labeled by incubation with 5 mM mBBr (Merk Millipore) in sample buffer during 2 h at room temperature in the dark. The excess of mBBr was removed by three washes with destaining solution (40% ethanol, 10% acetic acid) lasting 1 h, overnight and again 1 h. Fluorescent bands were visualized using a Gel-Doc (BioRad) with UV excitation (standard filters for ethidium bromide). Coomassie staining of the same gel was used to normalize fluorescence signals. Quantification of the bands was done by densitometry using Quantity One. Fluorescence signals coming from a replicate gel not treated with DTT were subtracted (**Supplementary Figure S2B**). When comparing oxidation of titin and myosin, we normalized the oxidation signals by their density of cysteines (Uniprot entries A2ASS6 and Q02566 for mouse cardiac titin and myosin, respectively). All gels in a comparative quantification were analyzed from the same unprocessed GelDoc image.

Mass spectrometry

Titin bands were sliced from SDS-PAGE gels used for fluorescence quantifications, diced and washed by incubation with 200 µl high purity water (Fluka CHROMASOLV™ LC-MS) for 10 min at 1200 rpm (4 times). The resulting gel pieces were dehydrated by 2 incubations with 100% acetonitrile and 1 incubation with 50 mM ammonium bicarbonate (pH 8.8) in acetonitrile (both incubations, 15 min shaking at 1200 rpm). After drying using a SpeedVac, the gel pieces were incubated with modified trypsin from porcine pancreas (Sigma Aldrich) in digestion buffer (10% acetonitrile in 50 mM ammonium bicarbonate, pH 8.8) for 2 h in ice to allow the diffusion of the inactive enzyme, and then at 37ºC overnight. Digested tryptic peptides were extracted with 1%

trifluoroacetic acid in acetonitrile (15 min incubation, 1200 rpm shaking) and dried. Finally, they were resuspended in 1% trifluoroacetic acid by pulse-vortexing and sonication, and desalted using OMIX commercial columns (Biomaster group). Peptides were then injected into a reversed phase C-18 nano-column (Acclaim PepMap RSLC, 75 μm internal diameter and 50 cm length), and eluted to be analysed in a hybrid quadrupole-Orbitrap Q Exactive mass spectrometer (Thermo Scientific) for protein identification. A continuous acetonitrile gradient consisting of 0-30% A for 120 min, 50-90% B for 3 min (A= 0.1% formic acid; B= 98% acetonitrile, 0.1% formic acid) at a flow rate of 200 nL/min was used to elute tryptic peptides from the nano-column to a nanospray emitter for real time ionization and induced fragmentation. High resolution mass spectra were acquired in a data-dependent manner with dynamic exclusion by combining a MS spectrum (from 400-1500 m/z, 120,000 resolution) followed by the MS/MS spectra (60,000 resolution) from the 15 most intense species. For protein identification, tandem mass spectra were extracted and charge state was deconvoluted by Proteome Discoverer 1.4.0.288 (Thermo Fisher Scientific). All MS/MS spectra were analyzed using SEQUEST (Thermo Fisher Scientific). Full proteome search databases (mouse: UniProtKB/Swiss-Prot April27_2016, 48736 sequences; human: UniProtKB/Swiss-Prot, November 2019, 74333 sequences) were supplemented with 116 cRAP proteins (common Repository of Adventitious Proteins, Global Proteome Machine). SEQUEST searches allowed two missed cleavages and used 20 ppm and 20 mDa precursor and fragment mass tolerances, respectively. NEM (+125.047679 Da)- or mBBr (+190.074228 Da)-modified cysteines, and oxidation of methionine were specified as variable modifications. In these initial searches, a target-decoy fixed value PSM validation strategy was used to filter peptides according to XCorr values (more than 1.2 in doubly-charged peptides, or more than 1.4 in triply-charged peptides for <5% FDR, and more than 1.42 in doubly-charged peptides, or more than 1.79 for triply-charged peptides for <1% FDR). Since the vast majority of the identified peptides belonged to titin in searches against full proteome databases, to optimize coverage of cysteine peptides we repeated the search using titin-only reduced search databases [36]. Peptide identifications were validated using Vseq, an in-house developed tool that evaluates the mass tolerance, intensity, fragmentation goodness and quantitative value of MS/MS scans [37]. Maximum matched ions

value for a sequence was calculated considering the number of residues multiplied by 2, to cover the complete theoretical length of the main fragmentation series B and Y. Since experiments were acquired using a label-free strategy and using HCD for ion-induced dissociation, we set a threshold of 25% minimum matched ions, which corresponds to at least 50% of the Y-HCD-enhanced fragmentation series. We also filtered peptide identifications according to their E-scores, which is defined as the dot product of the intensities for all matched ions regardless of their charge state. We applied an E-score threshold of > 0.01. We verified that none of the unidentified scans showing a very low XCorr and matched ions value was above this limit. To estimate final FDR values, we repeated the searches considering the same parameters against the corresponding decoy databases. FDR was below 2% in all cases. To minimize false positive detection of oxidized cysteines, we analyzed in parallel the same samples without including DTT in the derivatization reactions. For each sample, cysteine positions belonging to mBBr-peptides identified both in the –DTT and +DTT treated specimens were excluded from the analysis (27 ± 5% and 30 ± 4% of the oxidized cysteine-containing peptides identified in mouse and in human). In order to semi-quantitatively describe the landscape of identified cysteine redox states, we calculated a Redox Identification Index (RII) for each cysteine as follows:

$$RII = \frac{1\cdot(\#Ox) - 1\cdot(\#Red) + 0\cdot(\#Ox\&Red)}{\#Replicates} \qquad \textbf{Equation 1}$$

where *#Ox* and *#Red* are the number of replicates in which the cysteine is detected as oxidized or reduced, respectively, *#Ox&Red* is the number of replicates in which the cysteine is detected in both oxidized and reduced forms and *#Replicates* is the total number of replicates in which the cysteine is detected. As NEM- and mBBr-modified peptides might be detected with different efficiencies, due to different ionization and sampling during MS fragmentation, we followed a restrictive approach that simply took into account whether each cysteine was detected modified with NEM ans/or mBBr in each replicate sample. Therefore, RII can take ±1, ±2/3, ±1/3 and 0 values for cysteines identified in three replicates; ±1, ±1/2, and 0 for cysteines identified in two

replicates; and ±1 and 0 for cysteines identified in one replicate. Although the coarseness of RII values may lead to dispersion of experimental data due to missing identifications, we expect this effect to be averaged out when RII from multiple cysteine positions are analyzed together (see **Figure 3**). Indeed, we have calculated the global RII for each cysteine conservation category by counting and comparing all mBBr- and NEM-modified peptides of all cysteines belonging to each conservation category, a procedure that results in RII values that are very similar to the ones obtained by averaging individual RIIs (**Supplementary Table 1**). All raw data used for cysteine validation and RII calculations can be found in **Supplementary Files S2 and S3**.

Monte Carlo simulations

We constructed a simplified model of titin's I band to predict the length of the molecule under force upon redox modifications using Monte Carlo simulations [18, 19]. Simulations calculate the length of the two entropic regions of the protein (PEVK and N2Bus) and the Ig domains, according to the Freely Jointed Chain model of polymer elasticity and the Bell's model of force-dependent reactions (**Supplementary Note S1**). The length of the entropic regions and the number of Ig domains in each isoform were determined according to human titin sequence in Uniprot, further curated in [18]. Titin domains were classified according to their cysteine content and arrangement, which was used to determine the modifications they could be target of (**Supplementary Table S2**) and their mechanical and kinetic parameters (**Supplementary Tables S3-S6**). The constructed model was subject to an oscillating force protocol (triangular waves, 1 Hz, 10 ms simulation step) for 3 hours. Pilot simulations were also conducted using 1 ms simulation steps, leading to equivalent results. In the initial state all domains are folded. If oxidative modifications are present, we consider they occur at all potential target sites. In conditions involving disulfide bonds, all domains capable of disulfide isomerization contain the BG disulfide in the initial state [18]. We averaged 10 independent simulations for each condition. The code for the simulations and the subsequent analysis of the data was written in Igor Pro (Wavemetrics).

Statistics

Statistical tests were run using Graph Pad Prism 8.3.1 for Windows. To evaluate the tendency of different categories of cysteines to be oxidized (RII>0), we estimated the corresponding p-values using the hypergeometric distribution function implemented in Excel (Microsoft). Errors are given by SEM, unless indicated otherwise.

Acknowledgements

This work was supported by the *Ministerio de Ciencia e Innovación* grants BIO2014-54768-P, BIO2017-83640-P, RYC-2014-16604 to JAC and PGC2018-097019-B-I00 to JV, the Regional Government of Madrid grants S2018/NMT-4443 and PEJ16/MED/TL-1593 to JAC and the Instituto de Salud Carlos III (Fondo de Investigación Sanitaria grant PRB3 (PT17/0019/0003-ISCIII-SGEFI / ERDF, ProteoRed), and "la Caixa" Banking Foundation (project code HR17-00247) to JV. We acknowledge funding from the European Research Area Network on Cardiovascular Disease through grant MINOTAUR to SS (The Austrian Science Fund – FWF, I3301) and JAC (ISCIII-AC16/00045). The CNIC is supported by ISCIII, the *Ministerio de Ciencia e Innovación* and the Pro CNIC Foundation, and was a Severo Ochoa Center of Excellence (SEV-2015-0505). IMM was the recipient of a CNIC-ACCIONA Masters Fellowship and holds a fellowship from "La Caixa" Foundation (ID 100010434, fellowship code LCF/BQ/DR20/11790009). CSC is the recipient of an FPI-SO predoctoral fellowship BES-2016-076638. We thank Wolfgang A. Linke and Pablo García-Pavía for critical feedback. We are also thankful for the insights of three anonymous reviewers.

Author contributions

EHG and JAC conceived and led the project. EHG, IMM, CSC, MRP, DG and RPJ analyzed titin sequence. EHG, IMM, CSG, NV, DVC and CBC did in-gel determination of reversible cysteine oxidations. EHG, IMM, EBK, EC and JV did and analyzed mass spectrometry experiments. MA, SS, and PPR procured and characterized human heart samples. EHG, AFT, JV and JAC did statistical analysis of experimental data. IMM did Monte Carlo simulations. EHG, IMM and JAC drafted the manuscript with input from all authors.

Competing interests

The authors declare no competing interests.

Data and material availability

Data and materials are available on reasonable request to the corresponding authors. Mass spectrometry raw data have been deposited in PeptideAtlas (http://www.peptideatlas.org/, Identifier: PASS01609).

List of Supplementary Materials

Supplementary Files S1-S3 and Supplementary Information File including Supplementary Figures S1-S4, Supplementary Notes S1-S3, Supplementary Tables S1-S6 and Supplementary References.

References

1. Linke, W.A. and N. Hamdani, *Gigantic business: titin properties and function through thick and thin.* Circulation research, 2014. **114**(6): p. 1052-68.
2. Kötter, S., et al., *Titin-Based Cardiac Myocyte Stiffening Contributes to Early Adaptive Ventricular Remodeling After Myocardial Infarction.* Circulation Research, 2016(119): p. 1017-1029.
3. Hopf, A.-E., et al., *Diabetes-Induced Cardiomyocyte Passive Stiffening Is Caused by Impaired Insulin-Dependent Titin Modification and Can Be Modulated by Neuregulin-1.* Circulation Research, 2018. **123**(3): p. 342-355.
4. Freundt, J.K. and W.A. Linke, *Titin as a force-generating muscle protein under regulatory control.* J Appl Physiol, 2019. **126**(5): p. 1474-1482.
5. Anderson, B.R. and H.L. Granzier, *Titin-based tension in the cardiac sarcomere: Molecular origin and physiological adaptations.* Progress in Biophysics and Molecular Biology, 2012. **110**(2): p. 204-217.
6. Eckels, E.C., et al., *The Work of Titin Protein Folding as a Major Driver in Muscle Contraction.* Annu Rev Physiol, 2018. **80**: p. 327-351.
7. Herman, D.S., et al., *Truncations of Titin Causing Dilated Cardiomyopathy.* New England Journal of Medicine, 2012. **366**(7): p. 619-628.
8. Kellermayer, D., J.E. Smith, and H. Granzier, *Titin mutations and muscle disease.* Pflügers Archiv - European Journal of Physiology, 2019. **471**(5): p. 673-682.
9. Fatkin, D., et al., *Precision Medicine in the Management of Dilated Cardiomyopathy.* Journal of the American College of Cardiology, 2019. **74**(23): p. 2921.
10. Ware, J.S. and S.A. Cook, *Role of titin in cardiomyopathy: from DNA variants to patient stratification.* Nature Reviews Cardiology, 2018. **15**(4): p. 241-252.
11. Cuenca, S., et al., *Genetic basis of familial dilated cardiomyopathy patients undergoing heart transplantation.* The Journal of Heart and Lung Transplantation, 2016. **35**(5): p. 625-635.
12. Opitz Christiane, A., et al., *Developmentally Regulated Switching of Titin Size Alters Myofibrillar Stiffness in the Perinatal Heart.* Circulation Research, 2004. **94**(7): p. 967-975.

13. Freiburg, A., et al., *Series of exon-skipping events in the elastic spring region of titin as the structural basis for myofibrillar elastic diversity.* Circulation research, 2000. **86**(11): p. 1114-21.
14. Kruger, M., *Posttranslational Modification of the Titin Springs: Dynamic Adaptation of Passive Sarcomere Stiffness*, in *Cardiac Cytoarchitecture*, E. Ehler, Editor. 2015, Springer International Publishing. p. 109-124.
15. Li, H., et al., *Reverse engineering of the giant muscle protein titin.* Nature, 2002. **418**(6901): p. 998-1002.
16. Kellermayer, M.S. and L. Grama, *Stretching and visualizing titin molecules: combining structure, dynamics and mechanics.* J Muscle Res Cell Motil, 2002. **23**(5-6): p. 499-511.
17. Herrero-Galán, E., I. Martínez-Martín, and J. Alegre-Cebollada, *Redox regulation of protein nanomechanics in health and disease: Lessons from titin.* Redox Biology, 2019. **21**: p. 101074.
18. Giganti, D., et al., *Disulfide isomerization reactions in titin immunoglobulin domains enable a mode of protein elasticity.* Nat Commun, 2018. **9**(1): p. 185.
19. Alegre-Cebollada, J., et al., *S-glutathionylation of cryptic cysteines enhances titin elasticity by blocking protein folding.* Cell, 2014. **156**(6): p. 1235-46.
20. Loescher, C.M., et al., *Regulation of titin-based cardiac stiffness by unfolded domain oxidation (UnDOx).* Proceedings of the National Academy of Sciences, 2020: p. 202004900.
21. Tomin, T., et al., *Mass Spectrometry-Based Redox and Protein Profiling of Failing Human Hearts.* Int J Mol Sci, 2021. **22**(4).
22. Manteca, A., et al., *Mechanochemical evolution of the giant muscle protein titin as inferred from resurrected proteins.* Nat Struct Mol Biol, 2017. **24**(8): p. 652-657.
23. Grutzner, A., et al., *Modulation of titin-based stiffness by disulfide bonding in the cardiac titin N2-B unique sequence.* Biophys J, 2009. **97**(3): p. 825-34.
24. Avner, B.S., et al., *Myocardial infarction in mice alters sarcomeric function via post-translational protein modification.* Molecular and Cellular Biochemistry, 2012. **363**(1-2): p. 203-215.
25. Bodi, B., et al., *Titin isoforms are increasingly protected against oxidative modifications in developing rat cardiomyocytes.* Free Radic Biol Med, 2017. **113**: p. 224-235.
26. Paulech, J., N. Solis, and S.J. Cordwell, *Characterization of reaction conditions providing rapid and specific cysteine alkylation for peptide-based mass spectrometry*. Biochimica et Biophysica Acta (BBA) - Proteins and Proteomics, 2013. **1834**(1): p. 372-379.
27. Xiao, H., et al., *A Quantitative Tissue-Specific Landscape of Protein Redox Regulation during Aging.* Cell, 2020. **180**(5): p. 968-983.e24.
28. Nedrud, J., et al., *Mechanics on Myocardium Deficient in the N2B Region of Titin: The Cardiac-Unique Spring Element Improves Efficiency of the Cardiac Cycle.* Biophysical Journal, 2011. **101**(6): p. 1385-1392.
29. Watanabe, D., C.R. Lamboley, and G.D. Lamb, *Effects of S-glutathionylation on the passive force–length relationship in skeletal muscle fibres of rats and humans.* Journal of Muscle Research and Cell Motility, 2019.
30. Mayans, O., et al., *Structural evidence for a possible role of reversible disulphide bridge formation in the elasticity of the muscle protein titin.* Structure, 2001. **9**(4): p. 331-40.
31. Hansen, R.E. and J.R. Winther, *An introduction to methods for analyzing thiols and disulfides: Reactions, reagents, and practical considerations.* Analytical Biochemistry, 2009. **394**(2): p. 147-158.
32. Rogers, L.K., B.L. Leinweber, and C.V. Smith, *Detection of reversible protein thiol modifications in tissues.* Anal Biochem, 2006. **358**(2): p. 171-84.
33. Rivas-Pardo, J.A., et al., *A HaloTag-TEV genetic cassette for mechanical phenotyping of proteins from tissues.* Nature Communications, 2020. **11**(1): p. 2060.
34. Wang, K., J. McClure, and A. Tu, *Titin: major myofibrillar components of striated muscle.* Proceedings of the National Academy of Sciences, 1979. **76**(8): p. 3698.

35. Lahmers, S., et al., *Developmental control of titin isoform expression and passive stiffness in fetal and neonatal myocardium.* Circulation research, 2004. **94**(4): p. 505-13.
36. Noble, W.S., *Mass spectrometrists should search only for peptides they care about.* Nature Methods, 2015. **12**(7): p. 605-608.
37. Cogliati, S., et al., *Mechanism of super-assembly of respiratory complexes III and IV.* Nature, 2016. **539**(7630): p. 579-582.
38. Kosuri, P., et al., *Protein folding drives disulfide formation.* Cell, 2012. **151**(4): p. 794-806.
39. Cazorla, O., et al., *Differential expression of cardiac titin isoforms and modulation of cellular stiffness.* Circ Res, 2000. **86**(1): p. 59-67.
40. Pajares, M., et al., *Redox control of protein degradation.* Redox Biology, 2015. **6**: p. 409-420.
41. Marino, S.M. and V.N. Gladyshev, *Cysteine Function Governs Its Conservation and Degeneration and Restricts Its Utilization on Protein Surfaces.* Journal of Molecular Biology, 2010. **404**(5): p. 902-916.
42. Verma, S., R. Dixit, and K.C. Pandey, *Cysteine Proteases: Modes of Activation and Future Prospects as Pharmacological Targets.* Frontiers in Pharmacology, 2016. **7**(107).
43. Giles, N.M., et al., *Metal and Redox Modulation of Cysteine Protein Function.* Chemistry & Biology, 2003. **10**(8): p. 677-693.
44. Mónico, A., et al., *Elucidating vimentin interaction with zinc ions and its interplay with oxidative modifications through crosslinking assays and molecular dynamics simulations.* bioRxiv, 2021: p. 2021.02.12.430929.
45. Bertoli, G., et al., *Two Conserved Cysteine Triads in Human Ero1α Cooperate for Efficient Disulfide Bond Formation in the Endoplasmic Reticulum.* Journal of Biological Chemistry, 2004. **279**(29): p. 30047-30052.
46. Klomsiri, C., P.A. Karplus, and L.B. Poole, *Cysteine-Based Redox Switches in Enzymes.* Antioxidants & Redox Signaling, 2010. **14**(6): p. 1065-1077.
47. Swain, L., et al., *Redox Imaging Using Cardiac Myocyte-Specific Transgenic Biosensor Mice.* Circulation Research, 2016. **119**(9): p. 1004-1016.
48. Kojer, K. and J. Riemer, *Balancing oxidative protein folding: The influences of reducing pathways on disulfide bond formation.* Biochimica et Biophysica Acta (BBA) - Proteins and Proteomics, 2014. **1844**(8): p. 1383-1390.
49. Riemer, J., N. Bulleid, and J.M. Herrmann, *Disulfide formation in the ER and mitochondria: two solutions to a common process.* Science, 2009. **324**(5932): p. 1284-7.
50. Saaranen, M.J. and L.W. Ruddock, *Disulfide Bond Formation in the Cytoplasm.* Antioxidants & Redox Signaling, 2012. **19**(1): p. 46-53.
51. Chung, H.S., et al., *Cysteine oxidative posttranslational modifications: emerging regulation in the cardiovascular system.* Circ Res, 2013. **112**(2): p. 382-92.
52. Cuello, F., et al., *Oxidation of cardiac myofilament proteins: Priming for dysfunction?* Molecular Aspects of Medicine, 2018. **63**: p. 47-58.
53. Santos, C.X.C., et al., *Redox signaling in cardiac myocytes.* Free Radical Biology and Medicine, 2011. **50**(7): p. 777-793.
54. Rivas-Pardo, J.A., et al., *Work Done by Titin Protein Folding Assists Muscle Contraction.* Cell Rep, 2016. **14**(6): p. 1339-47.
55. Brynnel, A., et al., *Downsizing the molecular spring of the giant protein titin reveals that skeletal muscle titin determines passive stiffness and drives longitudinal hypertrophy.* eLife, 2018. **7**: p. e40532.
56. Linke, W.A., et al., *Characterizing titin's I-band Ig domain region as an entropic spring.* Journal of Cell Science, 1998. **111**(11): p. 1567-1574.
57. Eckels, E.C., et al., *The Mechanical Power of Titin Folding.* Cell Rep, 2019. **27**(6): p. 1836-1847 e4.

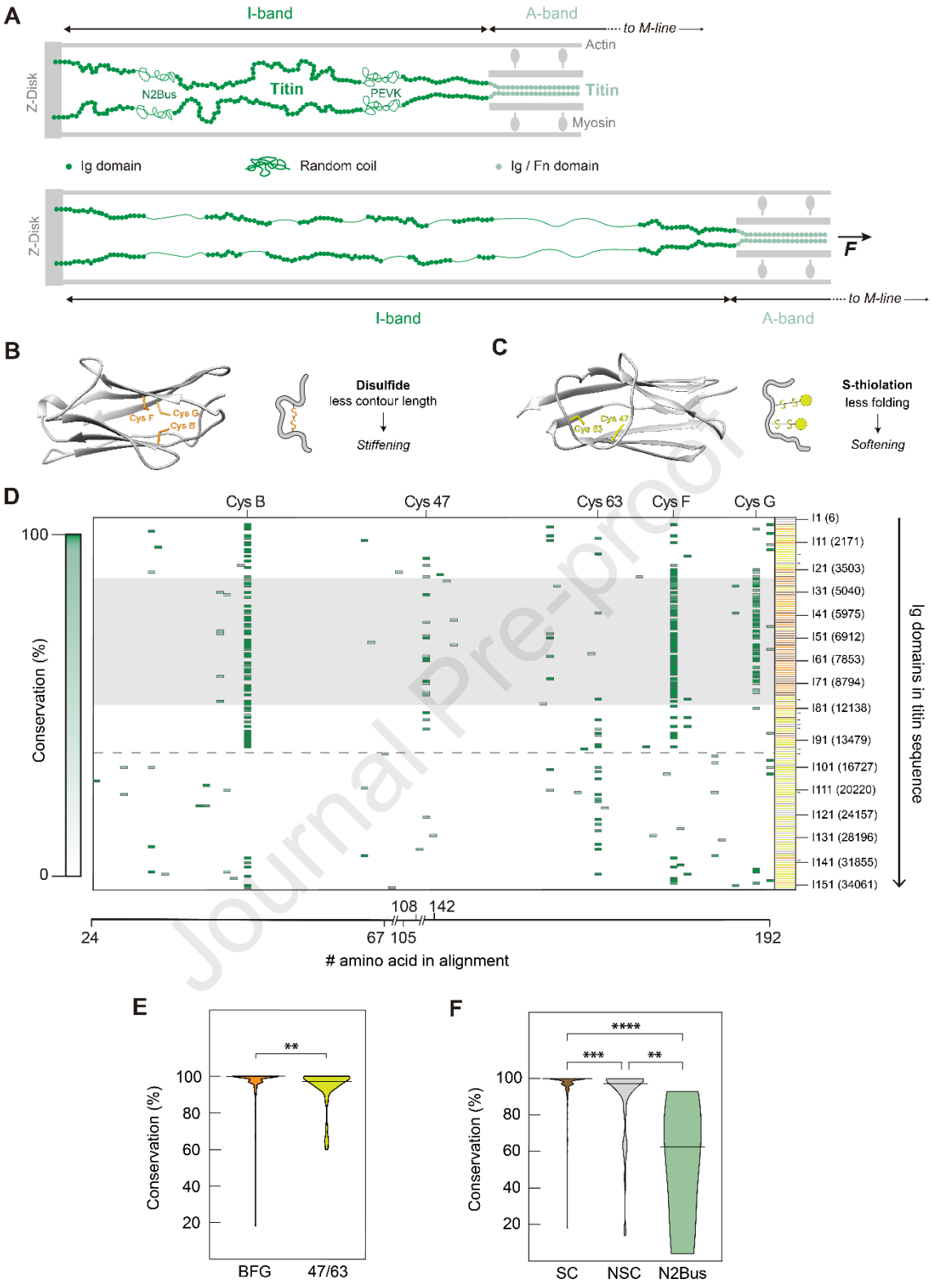

Figure 1. Structural and evolutionary conservation of titin mechanical cysteines. A: *Top:* Representation of half a sarcomere (not to scale), indicating the positions of the I-band (green) and the A-band (teal) of titin. Immunoglobulin-like (Ig), random-coil (PEVK and N2Bus) and fibronectin III (Fn) domains are shown. *Bottom*: Under mechanical force, the serially linked Ig

domains and the random coil regions extend, and Ig domains unfold. **B**: 3D homology model of an Ig domain containing the disulfide-competent CysB-CysF-CysG triad (I74, positions 9079-9168 from Uniprot entry Q8WZ42). The reduced contour length of the disulfide-containing unfolded state leads to domain stiffening. **C**: High-resolution structure of the traditionally named I27 domain of titin (also known as I91, PDB code 1tit), which contains unpaired, S-thiolation-competent cysteines 47 and 63 (positions 12674-12765 from Uniprot entry Q8WZ42). S-thiolations inhibit folding, leading to domain softening [19]. **D:** Map of cysteine positions along the alignment of Ig domains of human titin (breaks leave out Cys-free segments of the alignment). Structurally conserved positions B, 47, 63, F and G are indicated on top of the alignment. Positions are colored according to percentage of evolutionary conservation, from 0 (white) to 100% (dark green). The number and positions of Ig domains according to Uniprot Q8WZ42-1 (N2BA isoform) are indicated on the right. Pairs of dots mark Ig domains that are not annotated in Uniprot [18]. Ig domains are represented in grey if they are cysteine-free, in orange if they contain at least two of the triad, disulfide-competent cysteines B, F and G (disulfide-competent domains) [18], in yellow if they contain cysteines but no more than 1 cysteine B, F or G (domains incompatible with disulfide bond formation, only subject to potential S-thiolation), and in brown if at least two triad cysteines are present together with other cysteines (domains containing both disulfide-competent cysteines and cysteines that can only experience S-thiolation). The spliced-out region in the N2B titin isoform is indicated by the shaded grey area. The horizontal dashed line shows the boundary between the I- and A-band regions of titin (positions 14018-14019). **E**: Violin-plot distribution of percentages of evolutionary conservation of structurally conserved BFG (n=153) and 47/63 (n=40) cysteines in human titin. p(BFG *vs* 47/63)=0.0063 (Mann-Whitney). **F**: Violin-plot distribution of percentages of evolutionary conservation of structurally conserved (SC, including BFG and 47/63 cysteines, n=193), non-structurally conserved (NSC, n=113), and N2Bus (n=6) cysteines in human titin. p(SC *vs* NSC)=0.0001, p(SC *vs* N2Bus)<0.0001, p(NSC *vs* N2Bus)=0.0033 (Kruskal-Wallis and Dunn's multiple comparisons test). Evolutionary conservation values were calculated from the alignment of 36 titin sequences

from different species (**Supplementary Figure S1 and Supplementary File S1**). Horizontal bars in violin plots indicate median values.

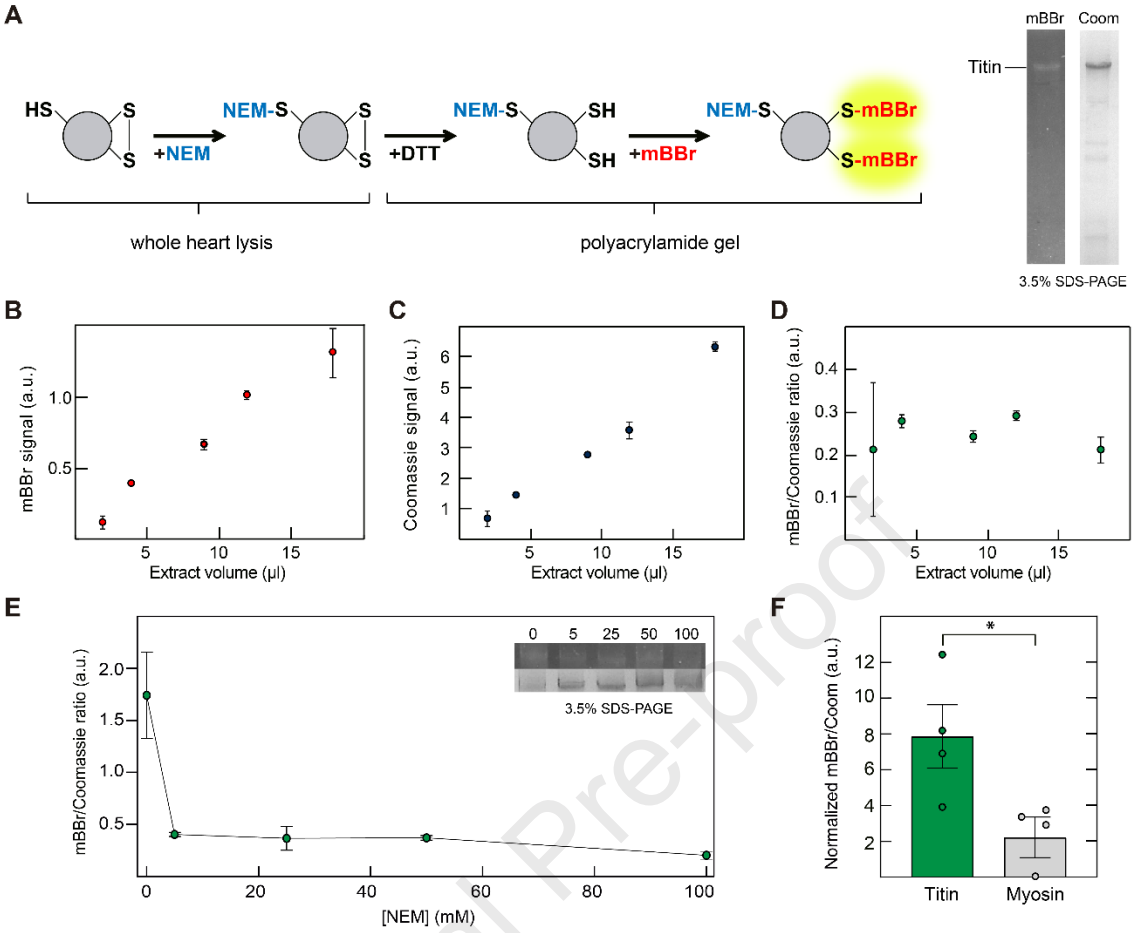

Figure 2. Titin is oxidized in basal conditions. A: *Left*: Reaction scheme to label reversibly oxidized thiols with mBBr. Protein extracts in which reduced thiols have been initially blocked by NEM are run in an SDS-PAGE gel. Following electrophoresis, oxidized thiols are reduced by DTT and then labeled with the fluorescent probe mBBr. *Right*: example SDS-PAGE gel used to quantify mBBr fluorescence from titin bands. Coomassie staining (Coom) of the same gel is used for normalization. **B, C**: The mBBr and Coomassie signals originating from titin are linearly dependent on the amount of lysate loaded in SDS-PAGE gels (all data points are the average of duplicates) (**Supplementary Figure S2A**). **D**: Final mBBr/Coomassie ratio is independent of the amount of lysate loaded in the gel. **E**: Scan to determine the concentration of NEM needed to completely block initially reduced titin thiols. Duplicates were performed for each NEM concentration. **F**: Quantification of the oxidation of titin and myosin in four different mouse hearts using 3.5% and 12% SDS-PAGE gels, respectively (see also **Supplementary Figure S2B**). The volume of lysate analyzed was adjusted so that both titin (15 µl) and myosin (3 µl) were in the

linear range of detection for Coomassie. Oxidation signal is normalized by the density of cysteines of each protein (13.3 Cys/1000 amino acids for titin, 7.2 Cys/1000 amino acids for myosin, see Methods). n =4 animals, p=0.0286 (Mann-Whitney).

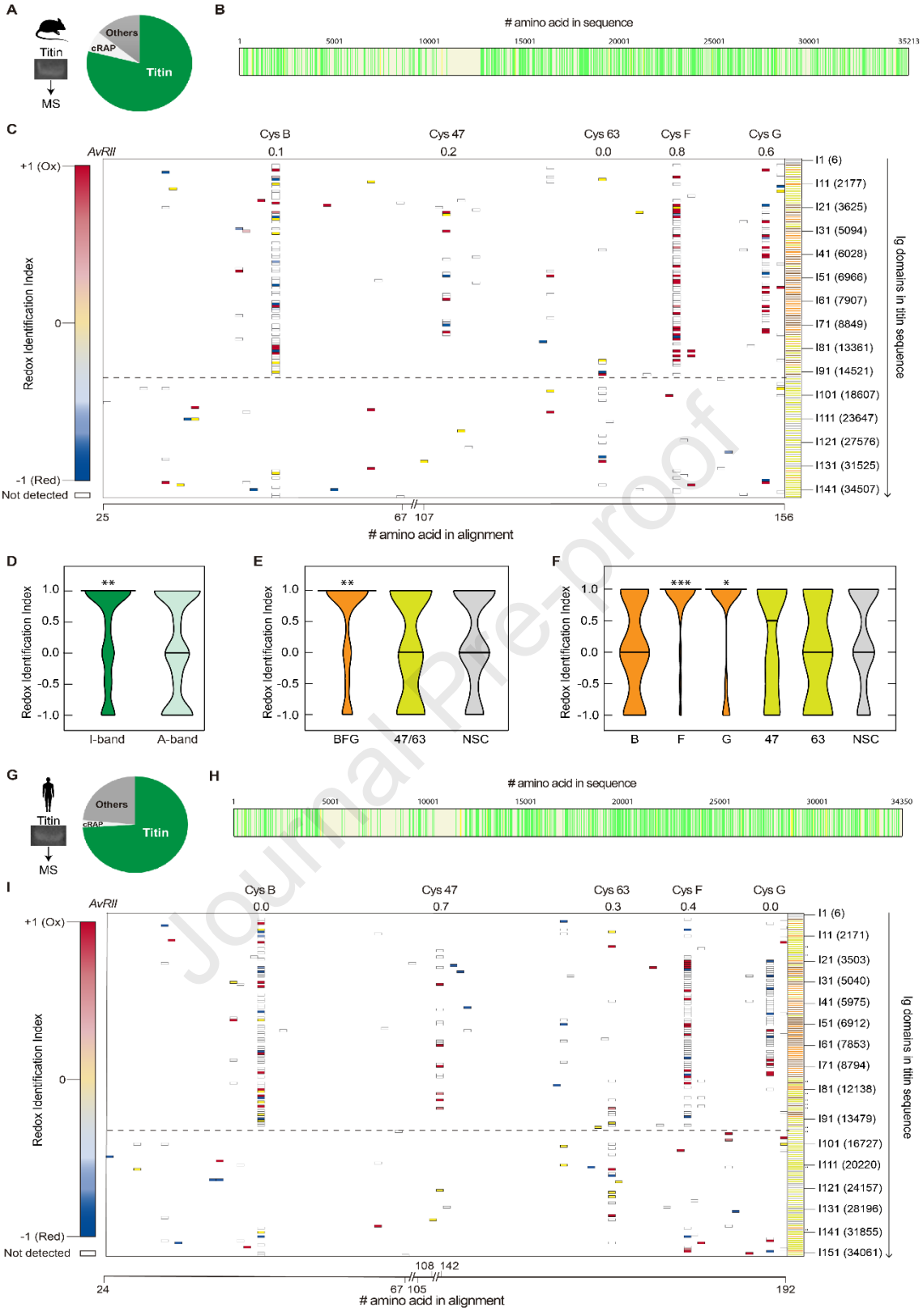

Figure 3. Landscape of cysteine oxidation in murine and human cardiac titin. **A**: Fraction of identified peptides belonging to murine titin (reference sequence Uniprot A2ASS6-1, which codes for the long N2BA titin isoform) when the MS/MS spectra are searched against a mouse proteome database containing common contaminants (cRAP). **B**: Aggregated titin coverage obtained after searching against the mouse proteome (n=3 mouse hearts; yellow and green, peptides detected with FDR<5% and <1%, respectively). **C**: Redox Identification Index (RII) map for every cysteine position in the alignment of Ig domains of mouse titin, according to the color code indicated on the left (red, oxidized; blue, reduced). Average RII (*AvRII*) for cysteines 47, 63 and the BFG triad across all Ig domains are indicated. Cysteines shown in white were not identified and do not contribute to RII calculation. The horizontal dashed line shows the boundary between the I- and A-bands of titin (positions 14880-14881 in Uniprot A2ASS6-1). The number and positions of Ig domains are indicated on the right. Ig domains are classified and colored as in Figure 1. **D**: Violin-plot distributions of RII for cysteines belonging to the I- (n=97) and A- (n=123) bands of murine titin. p(RII>0, I-band) = 0.0054, p(RII>0, A-band) = 0.9886 (hypergeometric test). **E**: Violin-plot distributions of RII for mouse titin cysteines BFG (n=61), 47/63 (n=14) and non-structurally conserved (NSC, n=33). p(RII>0, BFG) = 0.0054, p(RII>0, 47/63) = 0.8137, p(RII>0, NSC) = 0.9268 (hypergeometric test). **F**: Violin-plot distributions of RII for mouse cardiac titin cysteines B (n=21), F (n=23), G (n=17), 47 (n=8), 63 (n=6) and NSC (n=33). p(RII>0, B) = 0.9593, p(RII>0, F) = 0.0001, p(RII>0, G) = 0.0200, p(RII>0, 47) = 0.53365, p(RII>0, 63) = 0.7894, p(RII>0, NSC) = 0.9268 (hypergeometric test). Horizontal bars in violin plots indicate the median values. **G**: Fraction of identified peptides belonging to human titin (reference sequence Uniprot Q8WZ42-1, which corresponds to the long N2BA titin isoform) when the MS/MS spectra are searched against a database containing the human proteome and common contaminants (cRAP). **H**: Aggregated human titin coverage obtained after searching against the human proteome (left ventricular samples from 2 different non-transplanted non-failing donor hearts; yellow and green, peptides detected with FDR<5% and <1%, respectively). **I**: Redox Identification Index (RII) map for every cysteine position in the alignment of Ig domains of human titin, according to the color code indicated on the left (red, oxidized; blue, reduced).

Average RII (*AvRII*) for cysteines 47, 63 and the BFG triad across all Ig domains are indicated. Cysteines shown in white were not identified and do not contribute to calculation of RII. The dashed line shows the boundary between the I- and A-band regions of titin (positions 14018-14019 in Uniprot Q8WZ42-1). The number and positions of Ig domains are indicated on the right. Pairs of dots mark Ig domains that are not annotated in Uniprot. Ig domains are classified and colored as in Figure 1. **J**: Violin-plot distributions of RII for cysteines belonging to the I- (n=77) and A- (n=122) bands of human titin. p(RII>0, I-band) = 0.0435, p(RII>0, A-band) = 0.9220 (hypergeometric test). **K**: Violin-plot distributions of redox identification indexes for human titin cysteines BFG (n=57), 47/63 (n=16) and non-structurally conserved (NSC, n=33). p(RII>0, BFG) = 0.2746, p(RII>0, 47/63) = 0.0745, p(RII>0, NSC) = 0.8705 (hypergeometric test). **L**: Violin-plot distributions of redox identification indexes for cysteines B (n=25), F (n=20), G (n=12), 47 (n=7), 63 (n=9) and NSC (n=33) in human cardiac titin. p(RII>0, B) = 0.8974, p(RII>0, F) = 0.0093, p(RII>0, G) = 0.3537, p(RII>0, 47) = 0.0055, p(RII>0, 63) = 0.4759, p(RII>0, NSC) = 0.8705(hypergeometric test). Horizontal bars in violin plots indicate the median values.

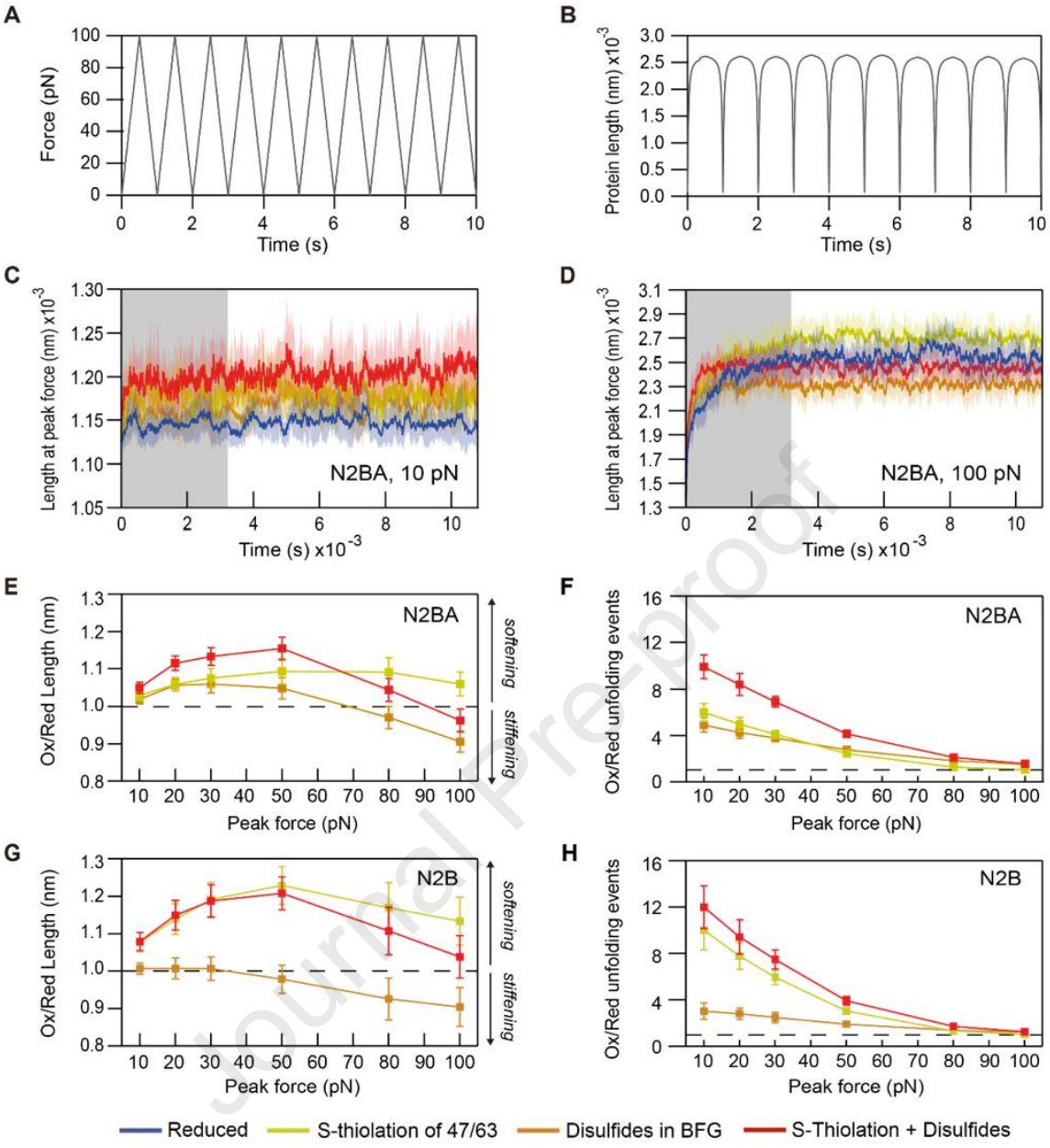

Figure 4. Effects of reversible cysteine oxidations on titin mechanics. A: Monte Carlo simulations subject virtual titins to a 1Hz oscillating triangular force pulse to a predefined peak force (100 pN in the example shown). **B**: Example of the length of reduced N2BA titin when pulled to a 100 pN peak force (10 seconds of simulation after reaching steady state are shown). **C,D**: Length of N2BA titin at peak force during simulations in which titin is reduced, or oxidized by disulfides, S-thiolation adducts or both (color code is indicated at the bottom; peak forces are indicated in the insets). The parameters of S-thiolations used in these simulations correspond to S-glutathionylations (**Supplementary Note S1**). Graphs show the average of 10 independent simulations and SD is indicated by shaded areas. For subsequent analyses, we

considered times longer than 1 hour, in which the length of titin fluctuates around steady state values (region outside the grey shading). **E**: Ratio of oxidized *vs* reduced N2BA titin length at different peak forces. **F**: Ratio of oxidized *vs* reduced N2BA unfolding events in simulations at different peak forces. **G**: Ratio of oxidized *vs* reduced N2B titin length at different peak forces. **H**: Ratio of oxidized *vs* reduced N2B unfolding events in simulations at different peak forces. In panels E-H, n= 10 simulations; error bars: SD. In panels E and G, the effect of the Ox/Red length on titin mechanics is indicated on the right.

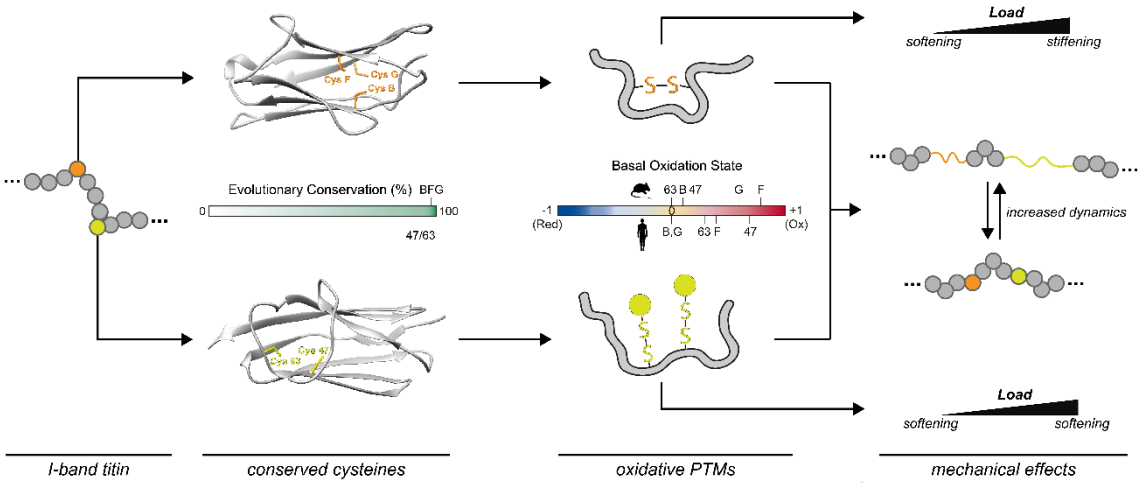

Figure 5. Oxidations of conserved cysteines enable mechanical modulation of titin. Structurally and evolutionary conserved cysteines B, F, G, 47 and 63 of Ig domains of the I-band of titin are oxidized in basal conditions. Mean evolutionary conservation percentages for cysteines BFG (98%) and 47/63 (94%) are shown on a conservation scale from 0 (white) to 100% (dark green). Average basal redox identification indexes for each individual cysteine are indicated on a scale ranging from -1 (always reduced) to +1 (always oxidized), both for mouse (above) and for human (below), as they appear on **Figure 3**. Disulfides (S-S) between cysteines belonging to the BFG triad soften titin at low forces and stiffen the protein at high forces, while S-thiolations (S-S-●) on cysteines 47 and 63 are always softening. Both types of oxidative posttranslational modifications (PTMs) increase the unfolding dynamics of Ig domains.

Declaration of interests

☒ The authors declare that they have no known competing financial interests or personal relationships that could have appeared to influence the work reported in this paper.

☐ The authors declare the following financial interests/personal relationships which may be considered as potential competing interests: